



An Ideal Two-Dimensional Porous B_4O_2 as Anode Material for Enhancing Ion Storage Performance

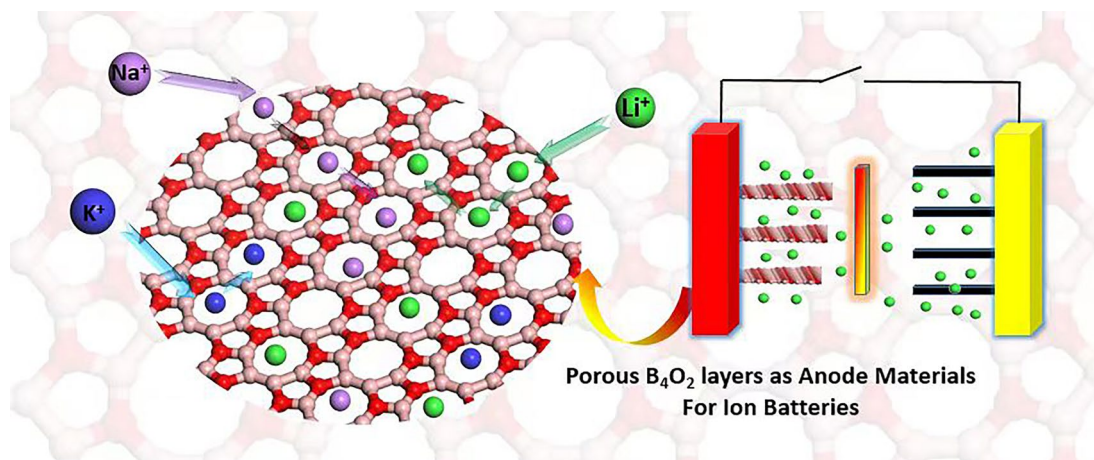
Chen Li^{1,2} · Yangtong Luo^{1,2} · Zhangyan Wang³ · Chengyong Zhong⁴ · Shuo Li²

Received: 30 June 2023 / Accepted: 2 October 2023 / Published online: 7 November 2023
© The Author(s) under exclusive licence to The Korean Institute of Metals and Materials 2023

Abstract

The utilization of two-dimensional porous materials as anodes in ion batteries has garnered significant interest within the field of clean energy because of their flexible architecture, high conductivity, rapid diffusion process and high specific ion capacity. Herein, we developed a new metal-free 2D porous compound, namely, B_4O_2 . The stability of the B_4O_2 monolayer was verified through the ab-initio molecular dynamics simulations and phonon spectrum calculations. The results demonstrate that the adsorption of K, Na, and Li atoms onto the B_4O_2 monolayer surface is remarkably stable, with all three species exhibiting a shared diffusion path. Specifically, we found that the adsorption of K atoms on the B_4O_2 monolayer surpasses that of Na and Li atoms, and the diffusion of K atoms occurs at a faster rate than Na and Li atoms on the same monolayer surface. The maximum theoretical specific capacity of K^+ , Na^+ and Li^+ is calculated to be 626.1 mAh/g. In addition, the B_4O_2 monolayer retains good electronic conductivity and electron activity during the atomic adsorption processes. Based on our findings, the B_4O_2 monolayer exhibits significant potential as anode material for ion batteries. This study paves the way for a novel approach in designing new 2D porous materials specifically tailored for energy storage and conversion applications.

Graphical Abstract



✉ Chengyong Zhong
zhongcy@cqu.edu.cn

✉ Shuo Li
lishuo@cdu.edu.cn

¹ School of Mechanical Engineering, Chengdu University, Chengdu 610106, People's Republic of China

² Institute for Advanced Study, Chengdu University, Chengdu 610106, People's Republic of China

³ College of Physical Education, Chengdu University, Chengdu 610106, People's Republic of China

⁴ College of Physics and Electronic Engineering, Chongqing Normal University, Chongqing 400047, People's Republic of China

Keywords 2D materials · Adsorption · Ion batteries · DFT · Energy storage

1 Introduction

In the field of energy technology, the study of high-performance energy storage systems continues to be a universally important and scientifically significant topic [1]. Lithium-ion batteries (LiIBs) have emerged as an excellent energy storage system for electronic devices [2]. However, with the rapid advancement of new energy vehicles, LiIBs are facing a number of challenges, including safety concerns, limited capacity and resource constraints [3, 4]. Currently, graphite remains the most commonly used anode material (AM) for LiIBs due to its cost-effectiveness and durability [5]. Nonetheless, the development of graphite as an AM for LiIBs is restricted by its theoretical capacity (372 mAh/g) [6]. Therefore, the search for and design of battery AMs with higher specific capacity and superior rate performance continues to be a formidable challenge.

K-ion batteries (KIBs) and Na-ion batteries (NaIBs) have gained increasing popularity because of their affordability, high energy density, and long lifespan [7]. In the case of NaIBs, M.K. Butt et al. predicted that 2D SnS could serve as a Na ion AM with high capacity (357 mAh/g), low open-circuit voltage (0.87 V) and low potential barrier (0.13 eV) [8]. Chen et al. experimentally developed a layer-mounted structure of nitrogen-doped carbon FeS-FeSe₂/NC, which exhibits great potential as an AM for NaIBs with high reversible capacity for Na ions (704.5 mAh/g) [9]. In the case of KIBs, Wu et al. experimentally prepared a composite structure of SnO₂ nanoparticles attached to the reduced graphene oxide. The incorporation of SnO₂ in this structure effectively improves the adsorption of potassium atoms and reduces the diffusion potential barrier of K⁺ for KIBs [10]. Based on these developments, NaIBs and KIBs are expected to emerge as the next generation of energy storage devices, potentially replacing LiIBs in the future.

The unique electrical, magnetic, optical, and catalytic properties of two-dimensional (2D) materials have led to their proposed applications in various fields, including electronics, spintronics, photoelectric devices, photo-electro-catalysts, energy storage, and energy conversion [11–17]. In particular, 2D materials possess several attractive properties for ion batteries, including large surface area, high conductivity and fast ion diffusion [18, 19]. These properties make them highly promising candidates for next-generation ion batteries. Numerous studies have demonstrated the excellent performance of 2D porous materials as AMs for LiIBs. For

instance, the 2D BSi monolayer exhibits not only a high specific capacity (689, 1034 and 1378 mAh/g), but also a low diffusion barrier (0.14, 0.24 and 0.37 eV) for KIBs, NaIBs and LiIBs, respectively [20]. The 2D Si₃C monolayer demonstrates a maximum specific capacity of 836, 1115 and 1394 mAh/g for KIBs, NaIBs and LiIBs, respectively. The K, Na, and Li atoms share similar diffusion paths on the Si₃C monolayer, with low diffusion barriers of 0.18, 0.34, and 0.47 eV, respectively [21]. The 2D GeSe monolayer demonstrates a maximum specific capacity of 353.65 mAh/g for K and Na ions, accompanied by low open circuit voltages (OCVs) of 0.030 and 0.219 V [22]. Additionally, the predicted PC₆ [23] and C₃N₃ [24] monolayers have also been investigated and shown to possess high performance as AMs for ion batteries. Therefore, it is evident that 2D materials utilized as AMs in ion batteries hold significant potential for energy storage and conversion applications.

The emergence of borophenes, a relatively new addition to the 2D material family, has garnered significant interest across the domains of chemistry, physics, and materials science [25–27]. The electron-deficient nature of boron allows for the formation of complex bonding configurations, giving rise to a wide range of borophenes with diverse structural and electronic properties [17, 28]. The structural flexibility of borophenes gives rise to a plethora of captivating physical and chemical properties, including extraordinary mechanical flexibility [29–31], magnetism [32, 33], superconductivity [34–36] and the ability to host Dirac cones [37, 38]. However, it is important to note that 2D materials are generally susceptible to oxidation in ambient conditions because of the prevalence of surface atoms [39]. Furthermore, our previous works predicted two type of borophene oxide: h-B₂O and t-B₂O, which exhibit novel electronic properties. Additionally, we found that oxygen atoms have a preference for incorporating into the basal plane of hexagonal borophene, instead of adopting the epoxide structure observed in silicene and graphene [15, 16].

Building upon the research on 2D materials as AMs in ion batteries and our prior investigations on 2D Boron oxide, we present a novel prediction of a 2D compound, B₄O₂, using CALYPSO computational method [40–42]. Our findings demonstrate that 2D B₄O₂ exhibits nonmagnetic semiconductor properties, possessing a band gap of 0.63 eV. To assess its potential as an AM for KIBs, NaIBs, and LiIBs, we further explored the diffusion and adsorption characteristics of K, Na, and Li atoms on B₄O₂ monolayers. The maximum theoretical specific capacity of K, Na, and Li on B₄O₂ was determined to be 626.1 mAh/g. Based on

these outcomes, we propose that 2D B_4O_2 holds promise as an electrode material for KIBs, NaIBs, and LiIBs.

2 Computational Methodology

All simulations were conducted by density functional theory (DFT) [43, 44] using the Vienna ab-initio Simulation Package (VASP). The interactions between electrons and ions were accurately predicted using the projector-augmented wave (PAW) method, while the Perdew–Burke–Ernzerhof (PBE) version of the generalized gradient approximation (GGA) [45] was utilized to account for exchange–correlation interactions among valence electrons. Van der Waals interactions were incorporated using the dispersion correction of DFT-D2 [46]. A plane-wave basis with a cutoff energy of 500 eV was employed. The Brillouin zone was represented by Monkhorst–Pack Γ k-point mesh of $3 \times 3 \times 1$ for structure relaxation and $7 \times 7 \times 1$ k-points for correct electronic properties. The atomic positions were optimized until the total energy converged within 10^{-5} eV and the maximum force reached 10^{-2} eV \AA^{-1} . To prevent interactions between periodically repeated layers, a vacuum of 15 \AA was introduced along the z axis. The climbing image nudged elastic-band (CI-NEB) method was applied to locate transition states [47–49]. The ab-initio molecular dynamics (AIMD) simulation was carried out at 300 K using a Nose–Hoover thermostat (NVT) ensemble [50, 51]. The VASPkit code was utilized for post-processing purposes [52].

The average adsorption energy (E_{ad}) of n ($X = K, Na$ or Li) atom on B_4O_2 monolayer is given by Eq. (1)

$$E_{ad} = \frac{(E_{nX/B_4O_2} - E_{B_4O_2} - nE_X)}{n} \quad (1)$$

where E_{nX/B_4O_2} is the total energies of nX atoms adsorbed on B_4O_2 monolayer, $E_{B_4O_2}$ is the total energies of B_4O_2 monolayer, E_X is the chemical potential of X bulk phases, and n is the number of adsorbates.

The theoretical specific capacity is calculated by Eq. (2)

$$C = n_{\max} F * \frac{(1000/3600)}{M} \quad (2)$$

where n_{\max} denotes the maximum number of adsorbed X atoms on B_4O_2 monolayer, F represents the Faraday constant, and M is the molar mass of B_4O_2 .

The OCV is calculated by Eq. (3)

$$OCV = \frac{(E_{B_4O_2} + nE_X - E_{nX/B_4O_2})}{ne} \quad (3)$$

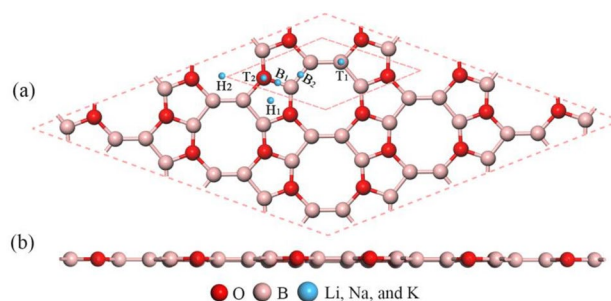


Fig. 1 Top **a** and side **b** views of the B_4O_2 monolayer. B, T, and H represent bridge, top, and hollow sites, respectively, for the possible adsorption sites of K, Na, and Li on the B_4O_2 monolayer. The unit cell and supercell are marked by the pink dotted lines

The charge density difference (CDD) is obtained as follows:

$$\rho = \rho(X/B_4O_2) - \rho(B_4O_2) - \rho(X) \quad (4)$$

where $\rho(X/B_4O_2)$ is the charge density of the X atom adsorbed on the B_4O_2 monolayer, $\rho(B_4O_2)$ and $\rho(X)$ are the charge densities of the correspondingly isolated B_4O_2 monolayer and X atom.

3 Results and Discussion

3.1 Structure of the B_4O_2 Monolayer

The estimated B_4O_2 monolayer exhibits a planar structure with a rhombus unit cell (Fig. 1). After structural optimization, its steady-state lattice parameters were determined to be $a = b = 5.41$ \AA . The B–O and B–B bonds in the B_4O_2 monolayer contain pentagonal and octagonal rings, resulting in a unique porosity structure. The AIMD simulations for the B_4O_2 monolayer at room temperature are validated its thermal stability (Fig. S1a). The phonon spectrum of the B_4O_2 monolayer displays no imaginary frequencies (Fig. S1b), indicating that the monolayer is naturally stable.

3.2 Adsorption of K, Na, and Li Atoms on the B_4O_2 Monolayer

Considering the size effect and the calculated quantities in our systems, we tested the E_{ad} values of K, Na, and Li atoms on the $2 \times 2 \times 1$, $3 \times 3 \times 1$, and $4 \times 4 \times 1$ supercell of the B_4O_2 monolayer, and the $3 \times 3 \times 1$ supercell was used for the following calculations. Six possible sites (including the hollow, top, and bridge sites) for K, Na, and Li atoms adsorbed on the B_4O_2 monolayer (Fig. 1). The most stable adsorption site for K, Na, and Li on the B_4O_2 monolayer is the H_2 sites. The E_{ad} values of K, Na, and Li atoms on the B_4O_2 monolayer

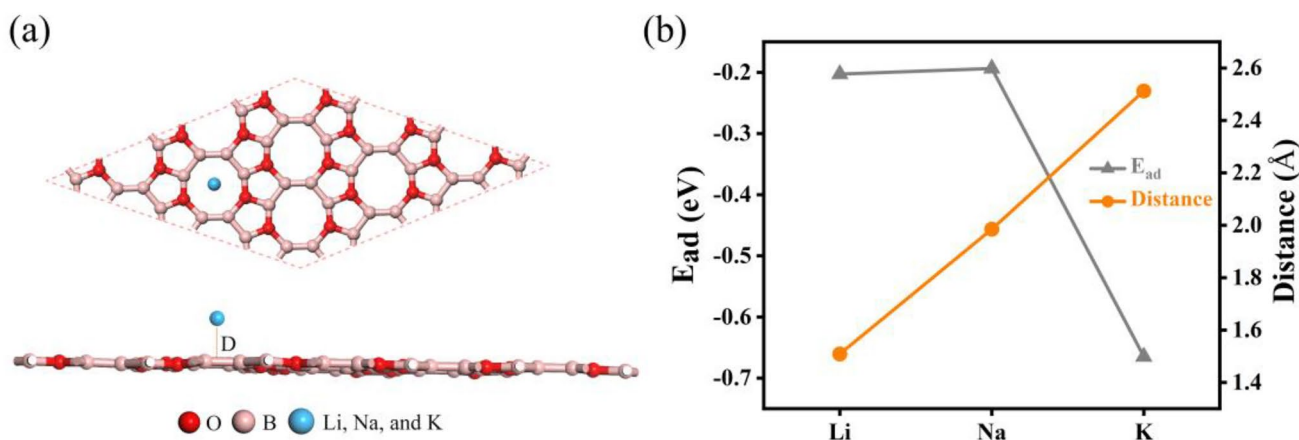


Fig. 2 **a** Top and side views of the most stable adsorption sites of K, Na, and Li atoms on the B_4O_2 monolayer, D is adsorption distance of atoms. **b** E_{ad} values and adsorption distances of K, Na, and Li atoms on the B_4O_2 monolayer

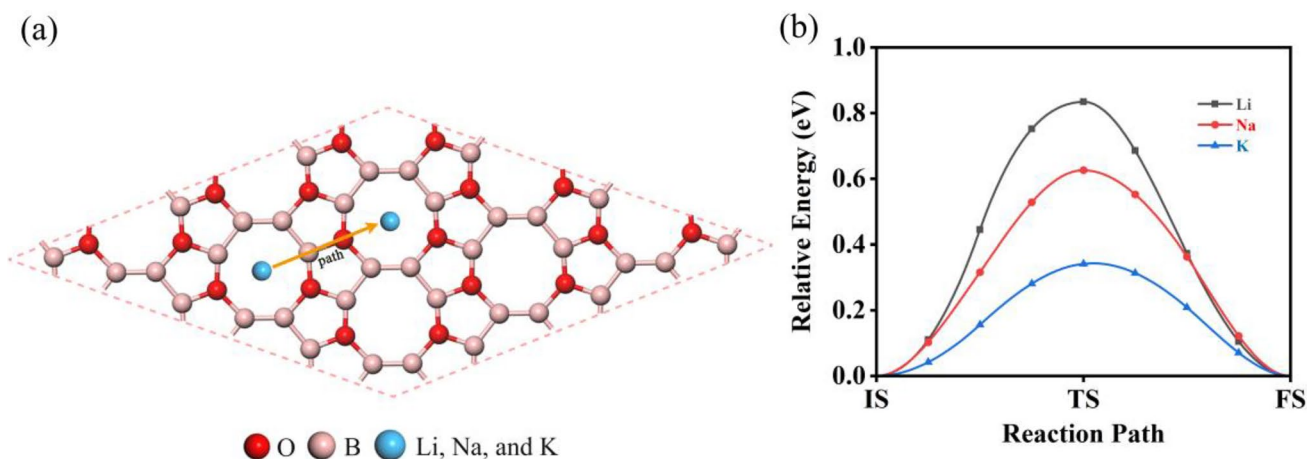


Fig. 3 **a** The diffusion pathways of K, Na, and Li on the B_4O_2 monolayer. **b** The energy barriers for K, Na, and Li on the B_4O_2 monolayer

(0.66, -0.19 and -0.20 eV for all) and their corresponding configurations are shown in Fig. 2. All E_{ad} values exhibit negative values, indicating a favorable and stable adsorption of K, Na, and Li atoms on the B_4O_2 monolayer. The E_{ad} for K atoms on the B_4O_2 monolayer is significantly higher compared to that of Na and Li atoms. This difference may be attributed to the influences of electronegativity and atomic radius [21]. Moreover, the E_{ad} values of Na and Li atoms on the B_4O_2 monolayer are lower than that of Li on the graphite (-0.26 eV) [53].

3.3 Diffusion of K, Na, and Li Atoms on the B_4O_2 Monolayer

In order to achieve high charge/discharge rates in practical ion batteries, rapid ion diffusion is a crucial characteristic that needs to be present [21]. As a consequence, we

computed the rate at which atoms of K, Na, and Li move from one H_2 site on the B_4O_2 monolayer to the other. Figure 3 shows the diffusion paths and the corresponding energy barriers. The energy barriers of diffusing K, Na, and Li atoms on a B_4O_2 monolayer are 0.34, 0.62, and 0.83 eV, respectively. The diffusion energy barrier of K in B_4O_2 monolayer is significantly reduced compared with Li and Na, but comparable to those of the 2D material GeC (0.33 eV) [54] and C-silicyne (0.34 eV) [55]. Consequently, the B_4O_2 monolayer exhibits a relatively low diffusion barrier for K atoms, facilitating rapid charging/discharging in K ion batteries. Moreover, the diffusion of K, Na, and Li atoms on the B_4O_2 monolayer is isotropic between these octagonal rings. This indicates that these ions can diffuse stably and flexibly on the B_4O_2 monolayer for the high charge/discharge rates that are required in practical ion batteries.

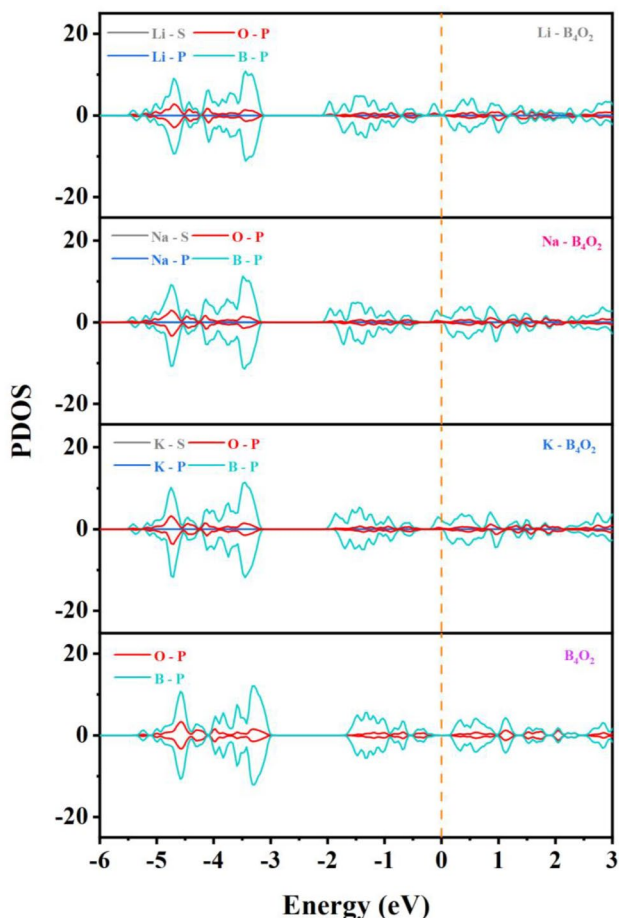


Fig. 4 PDOS of the freestanding B_4O_2 monolayer and K, Na, and Li atoms adsorbed on the B_4O_2 monolayer. The Fermi level was set to 0 eV with a dotted line

3.4 Electronic Properties

Charge transfer took place between K, Na, and Li ions and the B_4O_2 monolayer during both the adsorption and desorption processes. Consequently, the electronic characteristics of K, Na, and Li atoms adsorbed on the B_4O_2 monolayer are examined. Figure 4 displays the Total Density of States (PDOS) for the freestanding B_4O_2 monolayer and the adsorption of K, Na, and Li atoms onto the B_4O_2 monolayer. The B_4O_2 monolayer, which initially exhibits a semi-conducting nature, transitions into a metallic state upon the adsorption of K, Na, and Li atoms, owing to the transfer of charges from these atoms to the B_4O_2 monolayer. The metallic state of the B_4O_2 monolayer arises from the acquisition of electrons, resulting in the emergence of a new peak around the Fermi level. This phenomenon proves advantageous in maintaining excellent electrical conductivity for the anode.

To further understand the charge transfer among the substrate and adatoms, we can intuitively plot the CDD of K, Na, and Li atoms adsorbed on the B_4O_2 monolayer, (Fig. 5).

The electrons are depleting (blue) from K, Na, and Li atoms and accumulating (yellow) on the B_4O_2 monolayer. Furthermore, based on the Bader charge calculations, the charge transfer among K, Na, and Li atoms and the B_4O_2 monolayer is $1 e$, resulting in the ionic state of K, Na, and Li atoms, i.e. K^+ , Na^+ , and Li^+ . Furthermore, the transfer of charge can induce a spin-polarized state in the metallic B_4O_2 monolayer. This phenomenon suggests that when K^+ , Na^+ , and Li^+ ions are adsorbed, the electrical conductivity of the B_4O_2 monolayer is enhanced, resulting in a greater number of active electrons.

3.5 Theoretical Capacities

In addition, an excellent AM requires not only a low diffusion potential but also a high specific volume. Therefore, we conducted an investigation on different concentrations (1, 2, 4, 8, 18 atoms on the $3 \times 3 \times 1$ supercell) of K, Na, and Li atoms adsorbed on the B_4O_2 monolayer. The most stable configurations of these different concentrations are depicted in Fig. S2, where the ions were uniformly adsorbed on the H2 site of the B_4O_2 monolayer. The corresponding average E_{ad} values of K, Na, and Li atoms adsorbed on the B_4O_2 monolayer are presented in Fig. 6. The absolute values of the average E_{ad} decreased as the atomic concentrations increased, primarily due to the repulsive forces between atoms. Additionally, the change in average E_{ad} values for K atoms at different concentrations was more pronounced than that for Li and Na atoms, which may be explained by the larger radius of K atoms. The maximum number of K, Na, and Li atoms adsorbed on the B_4O_2 monolayer was found to be eighteen. Consequently, according to Eq. (2), the maximum theoretical storage capacity for K, Na, and Li atoms adsorbed on the B_4O_2 monolayer was calculated to be 626.1 mAh/g, surpassing that of other materials such as the black phosphorus monolayer (570 mAh/g) [56] and the FeSe monolayer (315 mAh/g) [57].

Furthermore, as the concentration of Li, Na, and K atoms increases, the geometric structure of the B_4O_2 monolayer undergoes deformation, as depicted in Fig. S2. This deformation occurs because of the charge transfer between the Li, Na, and K atoms and the B_4O_2 monolayer. The gain of electrons by the monolayer leads to its deformation as the charges redistribute. It is noteworthy that even at high adsorbent concentrations, the B_4O_2 monolayer remains stable. This phenomenon of deformation is not exclusive to the B_4O_2 monolayer but is also found in other 2D materials used as AMs, including Si_3C [21] and BP monolayer [56].

Fig. 5 Charge density difference (CDD) of Li **a**, Na **b**, and K **c** atoms adsorbed on the B_4O_2 monolayer, where yellow and blue indicate electron charge accumulation and dissipation, respectively. The isosurface is $0.0008 \text{ e}/\text{\AA}^3$

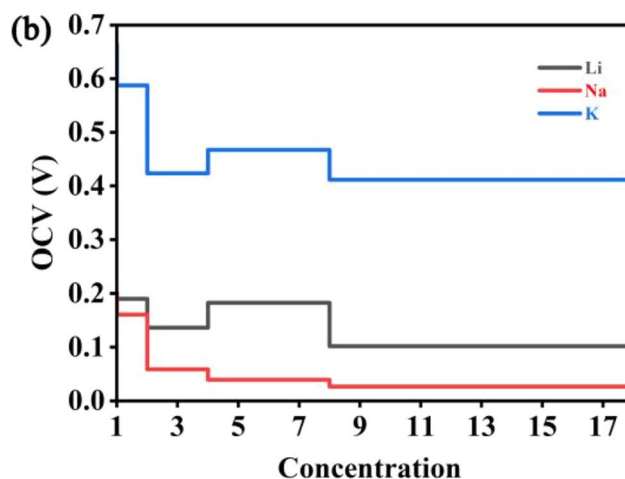
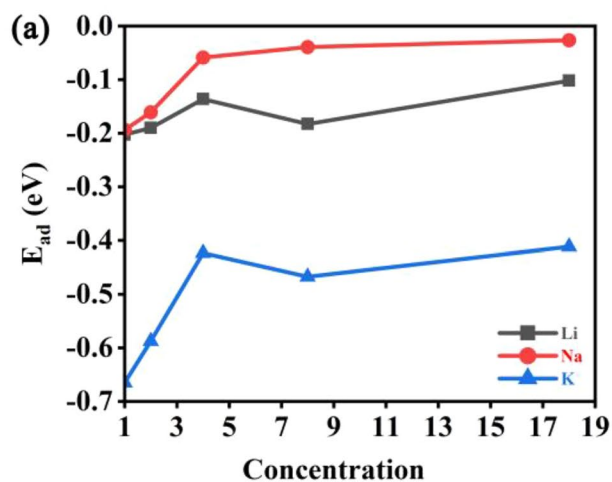
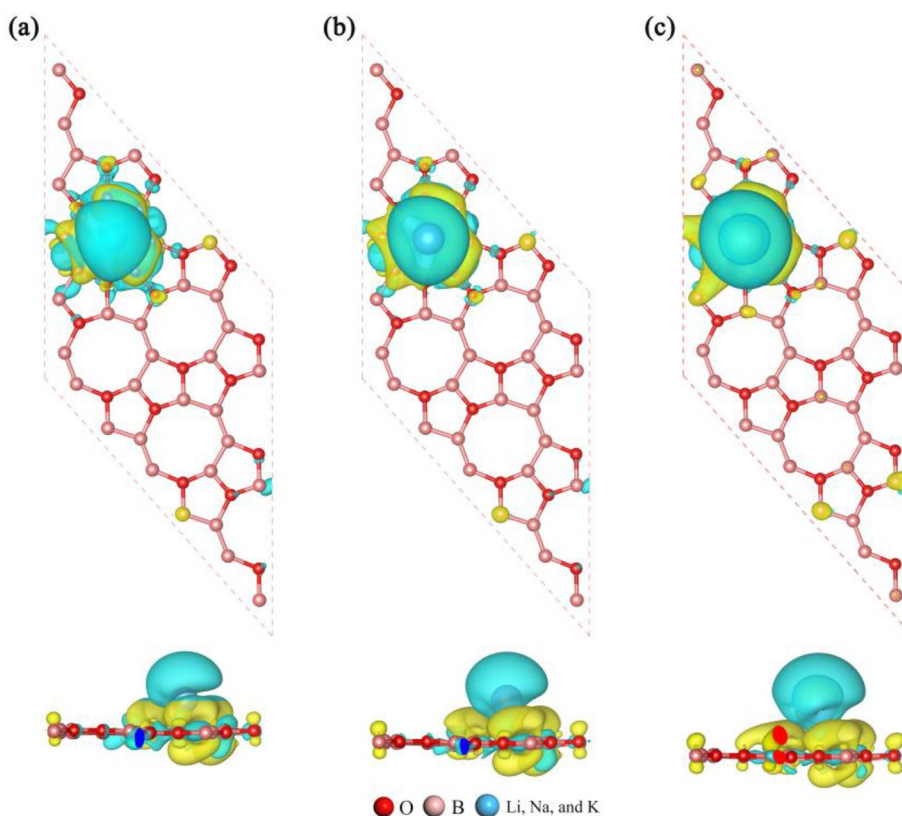


Fig. 6 **a** Average E_{ad} and **b** OCV of different concentrations of K, Na, and Li atoms adsorbed on the B_4O_2 monolayer

3.6 Open-Circuit Voltage

OCV is a crucial parameter that indicates the capacity of rechargeable Li-ion batteries [6]. In this study, we estimated the OCV using Eq. (3) and presented the results in Fig. 6. For Li on the B_4O_2 monolayer, the OCV is approximately 0.2 V at low concentrations but decreases to less than 0.1 V as the atomic concentrations increase.

The OCV for Na on the B_4O_2 monolayer remains very small, ranging from 0.03 to 0.05 V due to weak interaction. However, due to the strong interaction between K atoms and the B_4O_2 monolayer, the OCV for K on the B_4O_2 monolayer is increased compared to Li and Na. In general, a B_4O_2 monolayer with an OCV of less than 1 V [58, 59] has significant potential as a candidate for AMs in KIBs, NaIBs, and LiIBs.

4 Conclusion

Through spin-polarized DFT calculations, we conducted an assessment of the performance of 2D B₄O₂ monolayers as AMs for KIBs, NaIBs, and LiIBs. Our findings reveal that K, Na, and Li atoms can be stably adsorbed onto the surface of the B₄O₂ monolayer, with a negative E_{ad} of -0.66 , -0.19 and -0.20 eV for each atom. The most stable adsorption site is the octagonal rings formed by six B and two O atoms. While the diffusion pathways for K, Na and Li atoms on the B₄O₂ monolayer are the same, they exhibit different energy barriers of 0.34, 0.62 and 0.83 eV, respectively. The maximum theoretical specific capacity of K, Na, and Li ions on the B₄O₂ monolayer is calculated to be 626.1 mAh/g. This value surpasses the specific capacities of other AMs such as graphite (372 mAh/g) [60] and titanium dioxide (200 mAh/g) [61, 62]. Notably, this indicates that K possesses the same capacity as Li and Na and is comparatively easier to embed and delocalize. Additionally, the analysis of the electronic properties reveals that the B₄O₂ monolayers maintain good electronic conductivity and electron activity during the atomic adsorption processes. Our work not only demonstrates the potential of the B₄O₂ monolayer as a promising AM for KIBs but also paves the way for the development of novel 2D porous materials for future clean energy applications.

Supplementary Information The online version contains supplementary material available at <https://doi.org/10.1007/s13391-023-00465-w>.

Acknowledgements This work was supported by the start-up funding at Chengdu University.

Declarations

Competing Interest There are no conflicts to declare.

References

- Hong, X., Wang, R., Liu, Y., Fu, J., Liang, J., Dou, S.: Recent advances in chemical adsorption and catalytic conversion materials for Li–S batteries. *J. Energy Chem.* **42**, 144–168 (2020). <https://doi.org/10.1016/j.jechem.2019.07.001>
- Román-Ramírez, L., Marco, J.: Design of experiments applied to lithium-ion batteries: A literature review. *Appl. Energy* **320**, 119305 (2022). <https://doi.org/10.1016/j.apenergy.2022.119305>
- Kanimozhi, G., Naresh, N., Kumar, H., Satyanarayana, N.: Review on the recent progress in the nanocomposite polymer electrolytes on the performance of lithium-ion batteries. *Int. J. Energy Res.* **46**(6), 7137–7174 (2022). <https://doi.org/10.1002/er.7740>
- Evarts, E.C.: Lithium batteries: To the limits of lithium. *Nature* **526**(7575), S93–S95 (2015). <https://doi.org/10.1038/526s93a>
- Lim, Y.E., Choi, W.S., Kim, J.H., Ahn, Y.N., Kim, I.T.: The Sn–red P–Fe–based alloy materials for efficient Li–ion battery anodes. *J. Ind. Eng. Chem.* (2023). <https://doi.org/10.1016/j.jiec.2023.01.033>
- Khan, M.I., Nadeem, G., Majid, A., Shakil, M.: A DFT study of bismuthene as anode material for alkali-metal (Li/Na/K)-ion batteries. *Mater. Sci. Eng., B* **266**, 115061 (2021). <https://doi.org/10.1016/j.mseb.2021.115061>
- Zhang, L., Wang, W., Lu, S., Xiang, Y.: Carbon anode materials: a detailed comparison between Na-ion and K-ion batteries. *Adv. Energy Mater.* **11**(11), 2003640 (2021)
- Butt, M.K., Rehman, J., Yang, Z., Wang, S., El-Zatahry, A., Alofi, A.S.: Storage of Na in 2D SnS for Na ion batteries a DFT prediction. *Phys Chem Chem Phys* **24**(48), 29609–29615 (2022). <https://doi.org/10.1039/d2cp02780a>
- Chen, H., Lv, P., Liu, Q., Tian, P., Cao, S., Yuan, S.: Bonding iron chalcogenides in a hierarchical structure for high-stability sodium storage. *J. Colloid Interface Sci.* (2023). <https://doi.org/10.1016/j.jcis.2023.01.056>
- Wu, S., Feng, Y., Jiang, W., Wu, K., Guo, Z., Xiong, D., He, M.: Reduced graphene oxide coated modified SnO₂ forms excellent potassium storage properties. *Ceramics Int* (2023). <https://doi.org/10.1016/j.ceramint.2023.01.168>
- Schaibley, J.R., Yu, H., Clark, G., Rivera, P., Ross, J.S., Seyler, K.L., Xu, X.: Valleytronics in 2D materials. *Nat Rev Mater* **1**(11), 1–15 (2016). <https://doi.org/10.1038/natrevmats.2016.55>
- Deng, D., Novoselov, K., Fu, Q., Zheng, N., Tian, Z., Bao, X.: Catalysis with two-dimensional materials and their heterostructures. *Nat. Nanotechnol.* **11**(3), 218–230 (2016). <https://doi.org/10.1038/nnano.2015.340>
- Mao, J., Zhou, T., Zheng, Y., Gao, H.: Two-dimensional nanostructures for sodium-ion battery anodes. *J Mater Chem A* **6**(8), 3284–3303 (2018). <https://doi.org/10.1039/c7ta10500b>
- Xia, F., Wang, H., Xiao, D., Dubey, M., Ramasubramaniam, A.: Two-dimensional material nanophotonics. *Nat. Photonics* **8**(12), 899–907 (2014). <https://doi.org/10.1038/nphoton.2014.271>
- Zhong, C., Wu, W., He, J., Ding, G., Liu, Y., Li, D., Zhang, G.: Two-dimensional honeycomb borophene oxide: strong anisotropy and nodal loop transformation. *Nanoscale* **11**(5), 2468–2475 (2019). <https://doi.org/10.1039/C8NR08729F>
- Zhong, C., Feng, C.: An ideal two-dimensional nodal-ring semimetal in tetragonal borophene oxide. *Phys. Chem. Chem. Phys.* **23**(32), 17348–17353 (2021). <https://doi.org/10.1039/D1CP02003J>
- Lin, S., Guo, Y., Xu, M., Zhao, J., Liang, Y., Yuan, X., Li, Y.: AB 2 N monolayer: a direct band gap semiconductor with high and highly anisotropic carrier mobility. *Nanoscale* **14**(3), 930–938 (2022)
- Gao, S., Wei, F., Jia, B., Chen, C., Wu, G., Hao, J., Lu, P.: Two-dimensional van der Waals layered VSi₂N₄ as anode materials for alkali metal (Li, Na and K) ion batteries. *J Phys Chem Solid* **178**, 111339 (2023)
- Kasprzak, G.T., Szczesniak, R., Durajski, A.P.: Computational insight into bilayer NC7 anode material for Li/Na/Mg-ion batteries. *Comput. Mater. Sci.* **225**, 112194 (2023)
- Wang, S., Wu, Y., Ye, X., Sun, S.: Predict low energy structures of BSi monolayer as high-performance Li/Na/K ion battery anode. *Appl. Surf. Sci.* **609**, 155222 (2023). <https://doi.org/10.1016/j.apsusc.2022.155222>
- Wang, Y., Li, Y.: Ab initio prediction of two-dimensional Si₃C enabling high specific capacity as an anode material for Li/Na/K-ion batteries. *J Mater Chem A* **8**(8), 4274–4282 (2020). <https://doi.org/10.1039/c9ta11589g>
- Zhou, Y., Zhao, M., Chen, Z.W., Shi, X.M., Jiang, Q.: Potential application of 2D monolayer β-GeSe as an anode material in Na/K ion batteries. *Phys. Chem. Chem. Phys.* **20**(48), 30290–30296 (2018). <https://doi.org/10.1039/c8cp05484c>
- Yang, M., Kong, F., Chen, L., Tian, B., Guo, J.: Potential application of two-dimensional PC6 monolayer as an anode material in alkali metal-ion (Li, Na, K) batteries. *Thin Solid Films* (2023). <https://doi.org/10.1016/j.tsf.2023.139734>
- Xia, X., Yin, H., Zhang, Y., Huang, S.: Boron-doped g-CN monolayer as a promising anode for Na/K-ion batteries. *Surf Interf* **36**, 102479 (2023). <https://doi.org/10.1016/j.surfin.2022.102479>

25. Wang, Z.-Q., Lü, T.-Y., Wang, H.-Q., Feng, Y.P., Zheng, J.-C.: Review of borophene and its potential applications. *Front. Phys.* **14**, 1–20 (2019)
26. Xie, S.-Y., Wang, Y., Li, X.-B.: Flat boron: a new cousin of graphene. *Adv. Mater.* **31**(36), 1900392 (2019)
27. Li, D., Gao, J., Cheng, P., He, J., Yin, Y., Hu, Y., Zhao, J.: 2D boron sheets: structure, growth, and electronic and thermal transport properties. *Adv. Funct. Mater.* **30**(8), 1904349 (2020)
28. Wang, Q., Fan, G., Xu, H., Tu, X., Wang, X., Chu, X.: C-doped boron nitride nanotubes for the catalysis of acetylene hydrochlorination: a density functional theory study. *Mol. Catal.* **488**, 110853 (2020)
29. Wu, X., Dai, J., Zhao, Y., Zhuo, Z., Yang, J., Zeng, X.C.: Two-dimensional boron monolayer sheets. *ACS nano* **6**(8), 7443–7453 (2012)
30. Feng, B., Zhang, J., Liu, R.-Y., Iimori, T., Lian, C., Li, H.: Direct evidence of metallic bands in a monolayer boron sheet. *Phys. Rev. B* **94**(4), 041408 (2016)
31. Mu, Y., Chen, Q., Chen, N., Lu, H., Li, S.-D.: A novel borophene featuring heptagonal holes: a common precursor of borospherenes. *Phys. Chem. Chem. Phys.* **19**(30), 19890–19895 (2017)
32. Zhou, X.-F., Oganov, A.R., Wang, Z., Popov, I.A., Boldyrev, A.I., Wang, H.-T.: Two-dimensional magnetic boron. *Phys. Rev. B* **93**(8), 085406 (2016)
33. Tkachenko, N.V., Steglenko, D., Fedik, N., Boldyreva, N.M., Minyaev, R.M., Minkin, V.I., Boldyrev, A.I.: Superoctahedral two-dimensional metallic boron with peculiar magnetic properties. *Phys. Chem. Chem. Phys.* **21**(36), 19764–19771 (2019)
34. Penev, E.S., Kutana, A., Yakobson, B.I.: Can two-dimensional boron superconduct? *Nano Lett.* **16**(4), 2522–2526 (2016)
35. Gao, M., Li, Q.-Z., Yan, X.-W., Wang, J.: Prediction of phonon-mediated superconductivity in borophene. *Phys. Rev. B* **95**(2), 024505 (2017)
36. Zhao, Y., Zeng, S., Ni, J.: Superconductivity in two-dimensional boron allotropes. *Phys. Rev. B* **93**(1), 014502 (2016)
37. Feng, B., Zhang, J., Ito, S., Arita, M., Cheng, C., Chen, L.: Discovery of 2D anisotropic Dirac cones. *Adv. Mater.* **30**(2), 1704025 (2018)
38. Zhang, H., Xie, Y., Zhang, Z., Zhong, C., Li, Y., Chen, Z., Chen, Y.: Dirac nodal lines and tilted semi-Dirac cones coexisting in a striped boron sheet. *J. Phys. Chem. Lett.* **8**(8), 1707–1713 (2017)
39. Mannix, A.J., Kiraly, B., Hersam, M.C., Guisinger, N.P.: Synthesis and chemistry of elemental 2D materials. *Nat. Rev. Chem.* **1**(2), 0014 (2017)
40. Gao, B., Gao, P., Lu, S., Lv, J., Wang, Y., Ma, Y.: Interface structure prediction via CALYPSO method. *Sci. Bull.* **64**(5), 301–309 (2019). <https://doi.org/10.1016/j.scib.2019.02.009>
41. Wang, Y., Lv, J., Zhu, L., Ma, Y.: CALYPSO: A method for crystal structure prediction. *Comput. Phys. Commun.* **183**(10), 2063–2070 (2012). <https://doi.org/10.1016/j.cpc.2012.05.008>
42. Wang, Y., Lv, J., Zhu, L., Ma, Y.: Crystal structure prediction via particle-swarm optimization. *Phys. Rev. B* **82**(9), 094116 (2010). <https://doi.org/10.1103/PhysRevB.82.094116>
43. Kohn, W., Sham, L.J.: Self-consistent equations including exchange and correlation effects. *Phys. Rev.* **140**(4A), A1133 (1965). <https://doi.org/10.1103/physrev.140.a1133>
44. Hohenberg, P., Kohn, W.: Inhomogeneous electron gas. *Phys. Rev.* **136**(3B), B864 (1964). <https://doi.org/10.1103/PhysRev.136.B864>
45. Perdew, J.P., Burke, K., Ernzerhof, M.: Generalized gradient approximation made simple. *Phys. Rev. Lett.* **77**(18), 3865 (1996). <https://doi.org/10.1103/physrevlett.77.3865>
46. Grimme, S.: Semiempirical GGA-type density functional constructed with a long-range dispersion correction. *J. Comput. Chem.* **27**(15), 1787–1799 (2006). <https://doi.org/10.1002/jcc.20495>
47. Henkelman, G., Uberuaga, B.P., Jónsson, H.: A climbing image nudged elastic band method for finding saddle points and minimum energy paths. *J. Chem. Phys.* **113**(22), 9901–9904 (2000). <https://doi.org/10.1063/1.1329672>
48. Sheppard, D., Terrell, R., Henkelman, G.: Optimization methods for finding minimum energy paths. *J. Chem. Phys.* **128**(13), 134106 (2008). <https://doi.org/10.1063/1.2841941>
49. Henkelman, G., Jónsson, H.: Improved tangent estimate in the nudged elastic band method for finding minimum energy paths and saddle points. *J. Chem. Phys.* **113**(22), 9978–9985 (2000). <https://doi.org/10.1063/1.1323224>
50. Nosé, S.: A unified formulation of the constant temperature molecular dynamics methods. *J. Chem. Phys.* **81**(1), 511–519 (1984). <https://doi.org/10.1063/1.447334>
51. Hoover, W.G.: Canonical dynamics: Equilibrium phase-space distributions. *Phys. Rev. A* **31**(3), 1695 (1985). <https://doi.org/10.1103/physreva.31.1695>
52. Wang, V., Xu, N., Liu, J.-C., Tang, G., Geng, W.-T.: VASPKIT: A user-friendly interface facilitating high-throughput computing and analysis using VASP code. *Comput. Phys. Commun.* **267**, 108033 (2021). <https://doi.org/10.1016/j.cpc.2021.108033>
53. Peng, C., Mercer, M.P., Skylaris, C.-K., Kramer, D.: Lithium intercalation edge effects and doping implications for graphite anodes. *J. Mater. Chem. A* **8**(16), 7947–7955 (2020)
54. Ma, Y., Xu, S., Fan, X., Singh, D.J., Zheng, W.: Adsorption of K Ions on Single-Layer GeC for Potential Anode of K Ion Batteries. *Nanomaterials* **11**(8), 1900 (2021). <https://doi.org/10.3390/nano11081900>
55. Yadav, N., Chakraborty, B., Kumar, T.D.: First-principles study of a 2-dimensional C-silicene monolayer as a promising anode in Na/K ion secondary batteries. *Phys. Chem. Chem. Phys.* **23**(20), 11755–11763 (2021)
56. Jiang, H., Shyy, W., Liu, M., Wei, L., Wu, M., Zhao, T.: Boron phosphide monolayer as a potential anode material for alkali metal-based batteries. *J. Mater. Chem. A* **5**(2), 672–679 (2017). <https://doi.org/10.1039/c6ta09264k>
57. Lv, X., Li, F., Gong, J., Gu, J., Lin, S., Chen, Z.: Metallic FeSe monolayer as an anode material for Li and non-Li ion batteries: a DFT study. *Phys. Chem. Chem. Phys.* **22**(16), 8902–8912 (2020). <https://doi.org/10.1039/d0cp00967a>
58. Anasori, B., Lukatskaya, M.R., Gogotsi, Y.: 2D metal carbides and nitrides (MXenes) for energy storage. *Nat. Rev. Mater.* **2**(2), 1–17 (2017). <https://doi.org/10.1038/natrevmats.2016.98>
59. Winter, M.: J. O. Besenhard, ME Spahr and P. Novak. *Adv. Mater.* **10**, 725–763 (1998)
60. Persson, K., Sethuraman, V.A., Hardwick, L.J., Hinuma, Y., Meng, Y.S., Van Der Ven, A., Ceder, G.: Lithium diffusion in graphitic carbon. *J. Phys. Chem. Lett.* **1**(8), 1176–1180 (2010)
61. Lunell, S., Stashans, A., Ojamäe, L., Lindström, H., Hagfeldt, A.: Li and Na diffusion in TiO₂ from quantum chemical theory versus electrochemical experiment. *J. Am. Chem. Soc.* **119**(31), 7374–7380 (1997)
62. Olson, C.L., Nelson, J., Islam, M.S.: Defect chemistry, surface structures, and lithium insertion in anatase TiO₂. *J. Phys. Chem. B* **110**(20), 9995–10001 (2006)

Publisher's Note Springer Nature remains neutral with regard to jurisdictional claims in published maps and institutional affiliations.

Springer Nature or its licensor (e.g. a society or other partner) holds exclusive rights to this article under a publishing agreement with the author(s) or other rightsholder(s); author self-archiving of the accepted manuscript version of this article is solely governed by the terms of such publishing agreement and applicable law.